Available online at www.sciencedirect.com
ScienceDirect
Powder Technology 177 (2007) 53–63
POWDER TECHNOLOGY
www.elsevier.com/locate/powtec

Shape and size of microfine aggregates: X-ray microcomputed tomography vs. laser diffraction

S.T. Erdoğan [a,*], E.J. Garboczi [a], D.W. Fowler [b]

[a] National Institute of Standards and Technology, Gaithersburg, MD 20899, United States
[b] The University of Texas at Austin, Austin, TX 78712, United States

Received 6 November 2006; received in revised form 16 February 2007; accepted 21 February 2007
Available online 28 February 2007

Abstract

Microfine rock aggregates, formed naturally or in a crushing process, pass a #200 ASTM sieve, so have at least two orthogonal principal dimensions less than 75 μm, the sieve opening size. In this paper, for the first time, we capture true 3-D shape and size data of several different types of microfine aggregates, using X-ray microcomputed tomography (μCT) with a voxel size of 2 μm. This information is used to generate shape analyses of various kinds. Particle size distributions are also generated from the μCT data and quantitatively compared to the results of laser diffraction, which is the leading method for measuring particle size distributions of sub-millimeter size particles. By taking into account the actual particle shape, the differences between μCT and laser diffraction can be qualitatively explained.

Keywords: X-ray microcomputed tomography; Laser diffraction; Shape analysis; Size distribution analysis; Spherical harmonic method; Microfine concrete aggregates

1. Introduction

The shape and particle size distribution (PSD) of aggregate particles used in concrete (sand, gravel; 0.2 mm to 15 mm) can affect various properties in the fresh and hardened states, particularly rheological and mechanical properties [1–5]. Microfine aggregates are aggregates, formed in the crushing process, that pass a #200 ASTM sieve, so have at least two orthogonal principal dimensions less than 75 μm, the sieve opening size. Using the measured results obtained later on, we found that the equivalent spherical diameter (ESD) of the microfine aggregates studied in this paper had ESD values less than about 100 μm. The ESD of an aggregate is the diameter of a sphere with equal volume. The influence of these finer particles on many properties can often be greater than that of larger particles, presumably because of their greater surface area. Microfines could possibly also influence the cement chemical hydration process in concrete by providing added surface for nucleation of crystalline hydration products. The shape and PSD of these particles are thus significant and require adequate mathematical characterization.

There exists no standard test to directly measure the shape of microfines. Several indirect tests, some of which are standard methods (ASTM C204, ASTM D3398), have been proposed to measure coarse and fine particle shape. Indirect tests include packing/filling tests [6], flow tests [7,8], settling tests [9], and 2-D imaging methods [10]. There is also no standard test that completely and satisfactorily measures the PSD of microfine aggregates. A round-robin test to measure the PSD of cement particles, which are similar but several times smaller on the average than usual microfine aggregates, sponsored by ASTM committee C01.25.01, found that the only standard method for determining the PSD of cements (ASTM C115) is limited in scope and the absence of a standard procedure covering the whole range of cement PSD has led to the use of widely varying measurement methods in the industry [11,12], with low-angle light scattering (laser diffraction (LD)) being the most commonly used method [12].

To date, there has been no direct imaging, in three dimensions, of microfine aggregate particles, although some of the data from

* Corresponding author.
E-mail address: sinan.erdogan@nist.gov (S.T. Erdoğan).

0032-5910/$ - see front matter © 2007 Elsevier B.V. All rights reserved.
doi:10.1016/j.powtec.2007.02.016

the authors' work, at a voxel size of 4 μm, has been reported [13]. This paper reports that a combination of X-ray microcomputed tomography (μCT), at a voxel size of 2 μm, and spherical harmonic analysis have been used successfully to determine the shape and size of a variety of microfine aggregates. The combination of spherical harmonics and X-ray computed tomography has been used before to determine the size and shape of coarse and fine aggregates [14–17]. Other mathematical analyses of particle shape are available [18]. X-ray microtomography (μCT) is a technique similar to CT, but operating at smaller length scales, which can yield three-dimensional visualizations of features in the interior of a specimen. It has previously been used to measure internal crack growth [19], observe early hydration properties [20], and measure the variation of porosity [21] in cementitious materials. Using specimens containing microfine aggregates embedded in a matrix, the shape, and subsequently the size of these particles can be determined in three dimensions, within the constraint of the voxel size used.

Direct μCT results, in combination with spherical harmonic techniques, are used in this paper to quantitatively compare to and evaluate the more indirect LD PSD results. LD is a practical method but has limited accuracy when used on non-spherical particles. Determination of the shape of the particles tested with LD and therefore the ability to correct LD PSD results is a subject of ongoing research [22–24]. Although particles of non-spherical, but regular shapes have been useful to test such shape correction methods, the need for three-dimensional shape analysis is evident and has been expressed [25].

Methods and results are presented in the following order. First, a brief introduction to the LD and μCT methods and their underlying assumptions and limitations are given. The development of a method for preparing microfine aggregate μCT specimens, which is a non-trivial task, is presented. Shape analysis concepts used in this paper are reviewed and the mineralogy of the aggregates tested is given. The shape and PSD results obtained using the two different methods are then provided, followed by a comparative discussion of these results.

2. Procedure and materials

2.1. X-ray μCT and spherical harmonics

μCT is similar to regular CT in that images of slices of a specimen can be obtained and processed to yield complete, three-dimensional renderings of microstructure. In our case, we have a matrix with embedded particles, so a complete, within the limitation of voxel size, three-dimensional rendering of particle size and shape is obtained for all the particles embedded in the matrix and that appear in the images. μCT is the extension of CT to specimens between 1 mm and 10 mm in size and creates cross-sectional images with pixel size approaching 1 μm. The geometry of illumination, X-ray energy range, and intensity requirements for μCT are well met by a synchrotron X-ray source. The μCT data presented here were collected at beamline X2B, at the National Synchrotron Light Source (NSLS), Brookhaven National Laboratory. There are benchtop-size scanners that can do similar imaging.

The specimen is subjected to X-rays from many angles by rotating the specimen through many (several hundred) small angular increments between 0 rad and π rad [26,27]. Reconstruction algorithms yield a sequence of 2-D gray level images (slices) perpendicular to the vertical axis of the cylindrical specimens that represent differences in the attenuation (which is dependent mostly on density) of different points within it. These slices can be computationally stacked to yield a 3-D view of the specimen. The vertical dimension of the voxels is usually identical to the lateral dimension. Particles are identified using a thresholding process based on their gray level difference (density difference) with the epoxy. At this stage, the shape of each particle is known in terms of a collection of voxels. The surface details of each particle are exact only to the voxel size, so that details at a finer length scale than the voxel size have been lost. Certain characteristics of the particle, such as volume and principal dimensions, can be calculated accurately by counting voxels [28] (within a few percent) but some others, such as surface area, cannot.

Spherical harmonic functions [14,16] generated using the μCT data can compute any geometric quantity of the particle, such as volume, surface area, and moment of inertia, which can be defined by integrals over the volume or over the surface, since the spherical harmonic expansion gives an analytical, differentiable mathematical form for the surface [16]. Storing spherical harmonic coefficients also has memory advantages over storing the location of surface voxels, since only up to at most $n=N$ spherical harmonic coefficients need to be stored, which implies storing $(N+1)^2$ complex numbers. The maximum value of N that has been found to be needed for the gravel, sand, and microfine aggregates studied thus far has been $N=30$ [15–17], and usually $N\approx 20$ is sufficient for accurate particle shape analysis.

X-rays with energies between 12 keV and 20 keV were used with a 5× lens in scanning the microfines presented in this paper. The slices obtained were (1024 × 1024) pixels, collected with a charge-coupled device camera (CCD), with a square pixel size of 2 μm or 4 μm. Most of the data presented in this paper had a pixel size of 2 μm. Data acquisition time per sample was 1 h to 3 h (depending on the scan height) including image reconstruction. Image processing and spherical harmonic analysis required roughly 4 h per sample, each of which contained several thousand particles, using a single central processor unit.

2.2. Laser diffraction

Light waves striking a particle can be scattered, diffracted, or absorbed. Reflected and refracted lights make up the scattered light, and are affected by the form, size, and composition of the particles. Absorbed light is the incident light converted into heat and electrical energy and is dependent on size and composition [27]. Diffracted light is only dependent on the geometric shadow created by each particle in the light beam.

The complex refractive index of the material, $m=n+ik$ (where n is the real part and k the imaginary part), must in general be known to calculate the PSD of a sample based on the

diffraction pattern it produces, since scattering of light is due to differences in the refractive indices of the particle and the medium. The value of k is zero for non-absorbing, and 1 for completely absorbing materials. While values of n are available in the literature for many materials, values of k are more difficult to determine. Mie theory [29,30] is commonly used to interpret diffraction patterns and determine the PSD, and requires knowledge of the complex refractive index. Fortunately, the influence of absorption or refraction becomes less significant as the size of the particles increases relative to the wavelength of the incident light. For particles larger than about 5 times to 40 times the wavelength of the incident light, the Fraunhofer approximation [25], which only considers forward scattering and does not use the value of k, can be used to determine the PSD.

LD is performed as either dry analysis, in which the particles are dispersed in air, or wet analysis, in which microfines are suspended in water or other liquids. In the dry case, particles flow through (as an ensemble or cloud); and in the wet case, particles circulate through a broadened beam of laser light. Wet LD uses less than 1 g of material, while dry analysis uses tens of grams. The particles scatter the incident light onto a lens, which focuses the scattered light onto a detector array and a particle size distribution is calculated via inverting an integral equation constructed from the collected diffracted light data. There are many assumptions involved with Mie theory (or the Fraunhofer approximation) used for this interpretation [29].

Two assumptions are particularly important. The first is that particles are assumed to be spherical. LD is sensitive to the volume of the particle. For this reason, particle diameters are calculated from the measured volume of the particle, but assume a sphere of equivalent volume. The second is that the suspension is diluted and particle concentration is assumed to be so low that scattered radiation is directly measured by the detector (i.e. single scattering) and not rescattered by other particles before reaching the detector (i.e. multiple scattering).

The second assumption can be satisfied more easily by controlling the amount of microfine material used. The first one, however, is out of the control of the user, and it is clear that the results of this technique may be misleading, especially in the case of high percentages of flat and/or elongated particles being present in the sample [31]. This is analogous to sieve analysis yielding misleading results for elongated particles. Water is a good dispersant for microfine aggregates as there is little or no chemical interaction with water. In addition, ultrasonic energy is often used to break apart particle agglomerations. The time required to obtain a statistically sound PSD curve for one sample is about 20 min including setup, measurement, and cleanup. The reproducibility of LD results depends mostly on sampling practices, and is quite high, about 1% or better for the same sample.

2.3. Particle size distribution measurement by μCT and by LD

The μCT technique measures the volume of each particle, within the voxel size limits, and so it is possible to determine the PSD of the particles in the sample. A PSD curve is also generated by LD for a microfine sample. The PSD curves for microfines of the same type and source, taken from the same batch, measured using different techniques, will not necessarily be identical due to the different assumptions made in the different techniques. Another general assumption made, for any technique, is that the different samples analyzed, drawn from the same original batch of particles, are statistically identical, which is true for samples containing sufficiently large number of particles.

The typical PSD curve plots something like mass fraction, or number fraction, or volume fraction of particles against some measure of size. “Size” usually means a length that is characteristic in some way of the particles. Since μCT characterizes the true shape of a particle, and the spherical harmonic series gives an analytical, differentiable mathematical function for its surface, many lengths can be constructed, in addition to a particle’s principal dimensions, from its surface area, mean curvature, any order moment of the volume, and other geometric properties [15,16]. Any of these lengths are quantities that can be candidates for the abscissa for a PSD curve.

One possibility is to use the longest dimension (length, L) of the particles or, similarly, the shortest dimension (thickness, T). Using L will yield a PSD curve that is shifted towards larger particle “sizes” compared to a curve that uses the values of T to give a PSD curve. Another possibility is to use the intermediate dimension (width, W) of the particles. It has previously been suggested that the width distribution of particles obtained through image analysis is more closely correlated with the PSD obtained using sieve analysis [35], so the width distribution might be a reasonable way to determine PSD as compared to LD. One can also consider the case of observing multiple two-dimensional projections of a three-dimensional particle, in which case the maximum dimension of the average projection will be closer to the true width of the particle [15]. Yet another possibility is to use the ESD of the particles to draw the μCT PSD curve.

2.4. Sample preparation and scanning specifics for μCT

μCT, although similar to regular CT, is not as forgiving to poor sample preparation, due to the small length scales at which the imaging is performed. The specimen must be dimensionally stable and be able to withstand a high dose of X-rays. It is also important that there be a detectable absorption contrast, which in the case of aggregates requires that the microfines and the matrix in which they are embedded have sufficiently different densities. The selection of specimen size is driven by several criteria including absorption, contrast, and resolution. Approximately 90% of the incident radiation should be absorbed along the most radio-opaque path to obtain the best signal-to-noise ratio in the reconstructed image. This can be achieved by varying the sample thickness or the X-ray energy. The absorption of the X-rays (in the energy range used) is described by:

$$I/I_o = \mathrm{e}^{-\mu(\lambda)\rho \cdot x} \tag{1}$$

where I is the intensity of the absorbed X-ray beam, I_o is the intensity of the incident beam, ρ is the specimen density, x is the specimen thickness, and

$$\mu(\pi) = KZ^m\lambda^n \quad (2)$$

is the mass attenuation coefficient of the specimen where K is a constant that changes at each absorption edge, Z is the atomic number, m is approximately 4, λ is the X-ray wavelength, and n varies between 2.5 and 3.0 [27]. To absorb 90% of the incident radiation, the quantity $\mu(\lambda)\rho x$ should be approximately 2. Image noise or reconstruction artifacts result when the incident radiation absorbed deviates too much from 90%.

Unlike CT, magnification is selected by the choice of microscope objective. As magnification increases, the field of view decreases and the specimen dimension must be adjusted accordingly. Ideally, the entire specimen should be within the field of view of the CCD, as it is rotated during the scan (global scanning). With global scanning, there is the advantage that one can obtain a quantitative map of linear attenuation. When a part of the specimen extends beyond the field of view during rotation (local scanning), the image will have a relative grayscale in arbitrary units. However, this is not important in the case of scanning microfines for shape determination, but only if the density variation among or within the particles scanned is of interest. As a rule of thumb, the specimen size should not be greater than three times the field of view. The selection of specimen size, X-ray energy and resolution can also be driven by differences in X-ray absorption among the different components of the sample. If the contrast between the matrix and the aggregates is low, a lower X-ray energy and a smaller specimen will probably be needed. The concentration of the microfine particles in the specimen clearly is a factor influencing energy selection.

It is possible to prepare a microfine aggregate μCT specimen by simply filling a thin glass or other tube with the particles. However, this can make image processing more difficult due to a great number of particles in contact, thereby reducing the quality of the images and reducing the fine scale detail of the particles characterized. It is also desirable to avoid using an outer layer of material (the tube) through which the X-rays have to pass. Alternatively, the particles can be mixed with epoxy and cast in a small mold. The microfines scanned for this research were mixed with marine grade epoxy and cast in plastic cylindrical tubes with an inner diameter of approximately 2.5 mm. Any epoxy that will not creep after hardening and with a density contrasting with that of the aggregate can be used. It is important that the epoxy has sufficiently high yield stress to suspend the particles during hardening or, alternatively, that the mold is rotated continuously, otherwise the particles can settle and agglomerate. Due to the size of the opening of the mold, the epoxy–aggregate mixture was drawn into the mold using a suction bulb instead of being poured in. The outer plastic tubes peeled off the samples easily after the mixture set. Trials were also made using glass tubes with smaller inner diameters, but demolding was difficult as the epoxy tended to adhere to the inner glass surfaces. A cylindrical inner core section of the specimen was actually scanned in most cases, and therefore the slenderness of the sample was important mainly for minimizing the attenuation of the beam caused by the parts of the scan outside of the scan volume.

Different amounts (by mass fraction) of microfines were mixed with epoxy and trial scans revealed two important points. The first point is that it was useful to further sieve and separate the microfines to obtain clearer images with less background. When a large size range of particles is present, the smaller particles, which cannot be adequately resolved (those smaller than about five to ten times the voxel size), appear as blurred particles that complicate image processing. In the scans presented, the microfines were sieved into two groups; <38 μm (0–38) and 38 μm to 75 μm (38–75). The second point is that the amount of particles in the mixture should not exceed a volume fraction of about 15%. Although this value appears to be low, higher contents caused problems with image processing and a sufficient number of particles of a certain type can be characterized with one scan at this concentration. The heights of the specimens were 20 mm to 60 mm; however, this value can be much lower as the part of the specimen scanned was often less than 2 mm high.

It was observed that the mixing of the epoxy and the aggregate forms air bubbles that can be trapped in the specimen once the mixture has set. Such voids do not complicate the data acquisition or processing significantly because the density of air contrasts well with that of the aggregate or the matrix, and voids will appear very dark in the image; however, they can reduce the efficiency of the scan. Since the actual volume being scanned is rather small (several cubic millimeters), an air void can result in the wasting of valuable scan volume. It was found that slow mixing resulted in fewer air bubbles, and placing the samples in a vacuum for 2 min to 3 min eliminated any remaining large bubbles.

2.5. Concepts of shape analysis

The dimensions of irregularly shaped particles are usually defined via equivalent shape methods. Building equivalent shape models follows these steps: (1) one or more geometrical properties are selected, (2) the properties are measured by some means for the irregular particles, and (3) the dimensions of a regular shape are selected. The dimensions of the regular shape are determined by first equating the measured geometrical properties of the irregular shape to the analytically known geometrical properties of the regular shape, and then solving for the dimensions of the regular shape. This regular shape then becomes known as the "equivalent regular shape" particle that has the same selected geometrical properties as does the irregular shape.

One-parameter equivalent shapes are defined by only one geometrical property, two-parameter models by two geometrical properties, and so forth. An example of a one-parameter equivalent shape model is an equivalent volume sphere, whose diameter is determined by forcing the sphere to have the same volume as the irregular particle. This is probably the most used one-parameter model in particulate materials. Another one-parameter model, an equivalent surface area cube, would be defined by using a cube and forcing its surface area to be equal to that of the irregular particle. One-parameter models are of limited usefulness in describing the shape of irregular particles, for the following reason. If one constructs an equivalent volume

sphere, then an immediate question becomes: is any other geometrical property of the equivalent shape besides the volume at all close to that of the original irregular particle? For example, is the surface area of the equivalent volume sphere equal or close to that of the irregular particle? Usually the answer to this question is negative. One can use two or more parameter models. In Ref. [15]. three-parameter models were defined and investigated and shown to provide good predictions of other geometrical properties besides those that define their three parameters.

In Ref. [15], two three-parameter models were defined by choosing two regular objects with three dimensions: rectangular parallelepipeds (boxes), and tri-axial ellipsoids. All geometrical properties of both objects are totally defined by three lengths: a, b, and c, where the dimensions of the box are 2a, 2b, and 2c, and the semi-axes of the tri-axial ellipsoid are a, b, and c. One possible approach to define these three dimensions (L = length, W = width, T = thickness) for an irregular object is to measure the longest line within the body and to call this the "length" of the body L; then to find the longest such line that is orthogonal to L and to term it W. A similar procedure yields T, which has to be orthogonal to both L and T. This is essentially the procedure of the standard test ASTM D4791. For these microfine aggregates, the spherical harmonic-based mathematical approximation of the particle was used in a simple algorithm [15] to find approximations for L, W, and T simply by searching for pairs of surface points that satisfy the length and direction criteria. This is a well-defined and unique way to obtain three orthogonal dimensions from an irregular body, which can then be used to generate box or ellipsoid three-parameter equivalent shape models.

Other sets of three orthogonal dimensions can be defined via moments. It is known that all solid bodies possess a center of mass and a center of volume. These will be identical if the body is homogeneous in density or radially symmetric in both density and shape (rare in real particles). For convenience, we assume homogeneous density for the randomly-shaped microfine aggregates studied in this paper. This assumption is almost certainly not true in general [13], but it does not matter for the kind of shape determination analysis described herein, since we only really use the center of volume, not the center of mass. The coordinates of the center of volume of a solid body are given by:

$$X_i = \langle x_i \rangle_V \equiv \frac{1}{V}\int_V d^3r\ x_i \tag{3}$$

where V = the volume of the body, and the integral is taken over the entire volume of the body. In the spherical harmonic-based mathematical representation of the rock, the origin is taken at the center of volume, so that $X_1 = X_2 = X_3 = 0$. Measuring the coordinates of a point in the particle from this origin, one can then define the nth moment of x_i:

$$\langle (x_i)^n \rangle_V \equiv \frac{1}{V}\int_V d^3r (x_i)^n. \tag{4}$$

The most well known set of second moments ($n=2$) is probably the moment of inertia, or in this case, the moment of volume tensor, defined as a combination of various simpler moments:

$$I_{ij} = \left\langle r^2\delta_{ij} - x_i x_j \right\rangle_V \tag{5}$$

where $r^2 = (x_1)^2 + (x_2)^2 + (x_3)^2$, δ_{ij} is the Kronecker delta function (1 if $i=j$, 0 otherwise), and $x_1 = x$, $x_2 = y$, and $x_3 = z$. The moment of volume tensor can be diagonalized, and the diagonal elements are then called the principal moments of volume (PMV). The directions associated with these moments are orthogonal. The PMV then are three numbers that totally define the solid body's reaction to an applied torque, assuming that the body is rigid [32]. One can determine a three-parameter equivalent shape by equating the three PMV to the analytically known values for a tri-axial ellipsoid or a box [15].

2.6. Materials (microfine aggregates) tested

Four types of microfine aggregates were selected for measurement using the LD and μCT techniques. The specimens were selected to represent aggregates of different types and sources, on which a multitude of tests has already been conducted [33,34]. The source and primary mineral composition of the microfines, as found by X-ray diffraction (XRD), is given in Table 1.

Both laser diffraction and X-ray μCT were performed on powder selections that had been sieved in two ways: either <38 μm equivalent spherical diameter particles (e.g. MA 0–38) or 38 μm to 75 μm equivalent spherical diameter particles (e.g. MA 38-75).

3. Results

The shape analysis results are presented and discussed first, since the findings from these analyses will be used to understand the laser diffraction results.

The L, W, and T parameters were computed from the spherical harmonic surface reconstruction for the 38 μm to 75 μm particles with an uncertainty of about ±5 μm. The L, W, and T parameters were scaled by the T parameter to give normalized $\mathcal{L}$ ($=L/T$) and $\mathcal{W}$ ($=W/T$) values. Table 2 below gives a shape histogram for each of the four kinds of microfine aggregates that were listed in Table 1. The number percent of rocks falling into each bin is listed in Table 2, where $\mathcal{L}$ is along the horizontal axis and $\mathcal{W}$ is along the vertical axis in each histogram. In the MA histogram, for example, the $\mathcal{L}=2$–3 and $\mathcal{W}=1$–2 bin indicates that 33.4% of the MA particles, by number, had normalized values of L between 2 and 3 and

Table 1
The source and mineralogy of the microfine aggregates scanned [33]

Label	Description	XRD mineral identification	Source
MA	Marble	Calcite — $CaCO_3$	Maryland
PF	Limestone pond fines	Dolomite — $CaMg(CO_3)_2$	Ontario
NS	Natural stone	Dolomite — $CaMg(CO_3)_2$	Ontario
LS	Limestone	Calcite — $CaCO_3$	Michigan

Table 2
Shape histograms for the four types of microfine aggregates considered

MA 38–75						PF 38–75					
>5					0	>5					0
4–5				0	0	4–5				0	0
3–4			0.4	0.2	0.1	3–4			0.4	0	0
2–3		6.6	5.5	1.1	0.2	2–3		5.5	3.3	0.3	0
1–2	45.4	33.4	5.6	0.8	0.2	1–2	61.4	27.0	2.0	0.1	0
W / *L*	1–2	2–3	3–4	4–5	>5		1–2	2–3	3–4	4–5	>5

NS 38–75						LS 38–75					
>5					0	>5					0
4–5				0	0	4–5				0	0
3–4			0.2	0.1	0.1	3–4			0	0	0
2–3		5.2	3.2	0.5	0	2–3		2.5	1.5	0	0
1–2	55.9	32.2	2.4	0.2	0	1–2	64.3	30.0	1.3	0	0
	1–2	2–3	3–4	4–5	>5		1–2	2–3	3–4	4–5	>5

normalized values of W between 1 and 2. Entries above the diagonal are blank, since the relation $L \geq W$ must hold by definition. Note that larger entries along the horizontal direction indicate more prolate-shaped particles, while entries along the $L = W$ diagonal indicate more oblate-shaped particles. By this criterion, the MA aggregates appear to have somewhat more of a prolate character than do the other three aggregate types, since it has more weight along the $W = 1$ row and a smaller number in the $L = W = 1$ bin.

Table 3 shows the maximum, minimum, and average particle length-to-thickness ($\mathcal{L}$) and width-to-thickness ($\mathcal{W}$) ratios for the microfines. The numerical computation procedure enforces perpendicularity between the L, W, and T directions with an uncertainty of three degrees. With this uncertainty, the width will come out slightly smaller than the thickness a small fraction of 1% of the time. Therefore, the minimum W/T ratio is set to 1.00. Note that for the <38 μm class, only the particles with ESD above about 24 μm were used to compute the values of L, W, and T. Particles smaller than this were considered too small to give trustworthy surfaces for spherical harmonic analysis to be reliable. Their volumes were accurate to within 5%, however, so they could be used for PSD analysis (see Results section). The volumes of larger particles were accurate to about 1% [13]. Table 3 does show that, statistically, the two size classes for each kind of particle were somewhat similar to each other.

Table 3
The L/T and W/T aspect ratios for the microfines calculated from the μCT results

	MA 38–75		PF 38–75		NS 38–75		LS 38–75	
	$\mathcal{L}$	$\mathcal{W}$	$\mathcal{L}$	$\mathcal{W}$	$\mathcal{L}$	$\mathcal{W}$	$\mathcal{L}$	$\mathcal{W}$
Min	1.08	1.00	1.06	1.00	1.11	1.00	1.11	1.00
Max	8.24	3.46	4.84	3.46	4.78	3.64	3.82	2.86
Ave	2.25	1.58	1.98	1.50	2.04	1.51	1.89	1.37
	MA 0–38		PF 0–38		NS 0–38		LS 0–38	
	$\mathcal{L}$	$\mathcal{W}$	$\mathcal{L}$	$\mathcal{W}$	$\mathcal{L}$	$\mathcal{W}$	$\mathcal{L}$	$\mathcal{W}$
Min	1.11	1.00	1.09	1.00	0.99	1.00	1.10	1.00
Max	4.76	3.13	4.31	3.30	4.99	3.46	4.59	2.60
Ave	2.03	1.48	1.90	1.44	1.94	1.47	1.81	1.36

Studying Table 3, one could say that, for example, the average NS 38–75 microfine particle was roughly a 2:1.5:1 (length:width:thickness) prolate particle, which agrees well with its shape histogram in Table 2. The other particles give similar results, which is perhaps an indication of similar crushing processes. Table 3 indicates a tendency towards a prolate character for all four types of particles, with again the MA type having the highest prolate tendency, as was seen in Table 2.

Further shape analysis using a three-parameter box model was tried for these four microfine aggregates. Since in Ref. [15], a box model using the PMV lengths seemed to work the best for the microfine aggregates considered there, this model was used to analyze the microfines studied in this paper. For the 38–75 classes of particles, the PMV lengths were computed and used to generate a box model. The surface area and volume of this box model was computed, for every 38–75 class particle. These were graphed against the surface area and volume as computed directly from the μCT results. All four of the microfine aggregates were similar – Fig. 1 shows the results of this analysis for the MA 38–75 particles. The dashed lines are the lines of equality, so the equivalent shape box models work very well in predicting the volume and surface area of the particles.

Ref. [15] showed that the same kind of analysis could be done using the length, width, thickness (LWT) results, which gave a good linear correlation between the box predictions using the LWT numbers and the volume and surface area as computed by the μCT results. However, the slope of the linear

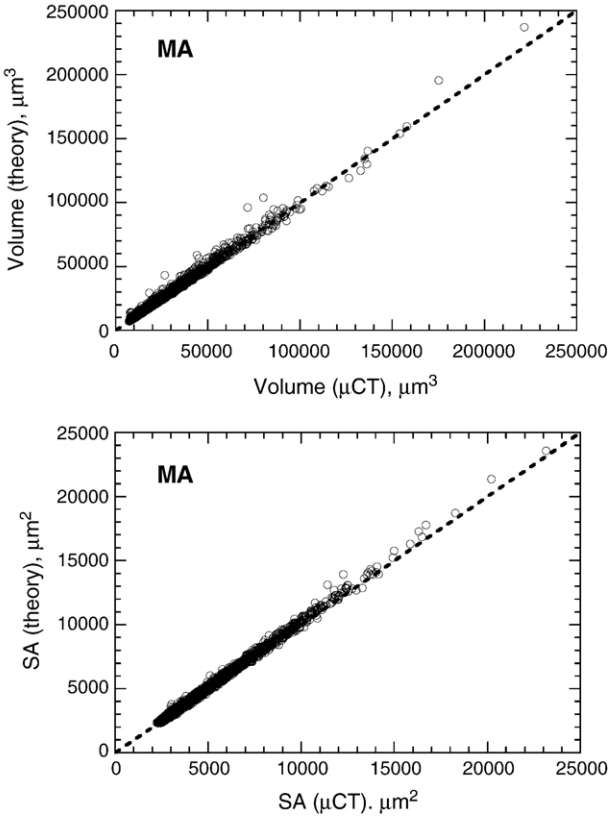

Fig. 1. Volume and surface area from the PMV box model vs. volume and surface area as computed directly from the μCT results.

correlation was not close to unity. This analysis was not done here, since the LWT parameters were not measured independently for these small particles. These parameters will be employed, however, in the following section on particle size distribution. On larger particles, *L*, *W*, and *T* could be measured directly, and so models using these parameters would be useful for predicting volume and surface area without having to resort to μCT measurements.

Since each microfine sample that was scanned only had particles that either passed, or were retained, on the #400 sieve (38 μm), the PSD results from the 0–38 and 38–75 specimens were compared to the LD PSD measured on these same kinds of sieved samples. The results from LD (percentages by mass of particles of a certain size) were adjusted to include only the particles with equivalent spherical diameter larger than 10 μm, since μCT could not resolve particles below about 10 μm. At the voxel size used, about 2 μm per voxel side, a 64 voxel particle had a volume of 512 μm^3 or an equivalent spherical diameter of about 10 μm. Particles below 64 voxels in volume are hard to distinguish from the noise in the original μCT image, so we chose to cut off the data at that point.

Fig. 2 shows the PSD curves obtained for the four different microfines, using the ESD, length, width, and thickness values from μCT. It is seen that, naturally, the thickness curves for all samples are to the left of (smaller particle size) the width curves, which in turn are to the left of the length curves. The ESD values for the particles scanned are between the thickness and the width curves. It is impossible to state that a single one of the parameters can provide an accurate PSD, for at least two reasons: (1) the correct PSD curve is not known, and (2) a single length parameter cannot really characterize a particle with random shape. The best choice of the length parameter may depend on the application for which the PSD curve is to be used. In regards to point (1), the μCT results are a direct measurement of the particle volumes, but there are probably not enough particles to be absolutely sure that we have obtained good statistics. In Fig. 3, it is clear that the μCT PSD curve drawn using the *L* data is by far the closest to the measured LD curve.

It was expected that the LD PSD results would not match the μCT PSD results, due to the many assumptions made in calculating the LD results, particularly the assumption of spherical particles. Calculating the PSD using the diffraction pattern created by a set of particles is not a trivial task [29], and it is not currently possible to analytically calculate the diffraction pattern of real particles or to back calculate the true shapes of real particles using real diffraction data. However, some regular but non-spherical shapes have been used to evaluate the influence of particle shape on PSD [25,36]. These results can help shed some light on our results. Mühlenweg and Hirleman [25] investigated the effect of ellipsoidal particle shape on diffraction patterns and the resulting PSD, using a geometrical optics approximation and Fraunhofer theory. Mie theory, which takes into account light absorption by the particles and therefore needs the imaginary part of the particle index of refraction, has to our knowledge only been worked out for spheres [29]. Mühlenweg and Hirleman exactly calculated the scattering, and then computed the PSD using a spherical assumption. They found that for particles with fixed ESD=20 μm, the calculated PSD changed as the particle shape became less and less spherical. For spheres, there essentially was a sharp spike centered at 20 μm, as would be expected. When the particles became 2:1 prolate ellipsoids of revolution, the apparent distribution of equivalent spherical sizes ranged from 13 μm to 31 μm, increasing to a distribution of apparent sizes ranging from 7.5 μm to 52 μm for a 5:1 prolate

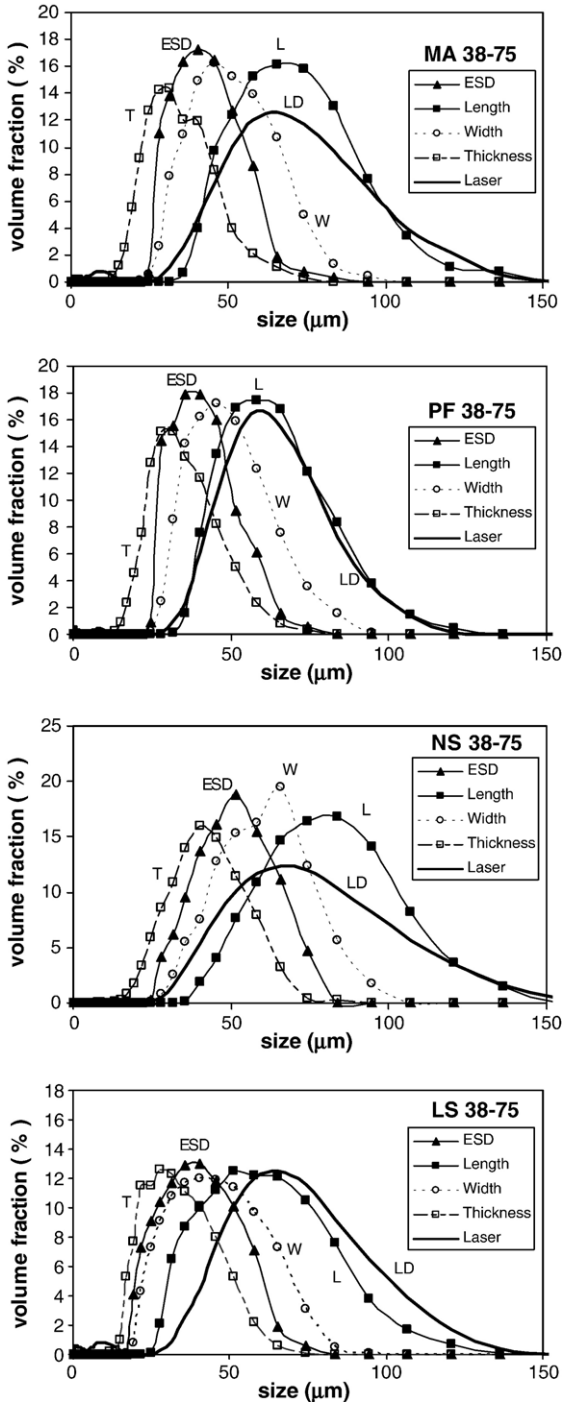

Fig. 2. PSD curves obtained for four different 38 μm to 75 μm microfines using wet laser diffraction (LD) and using the ESD, thickness (*T*), width (*W*), and length (*L*) values from μCT.

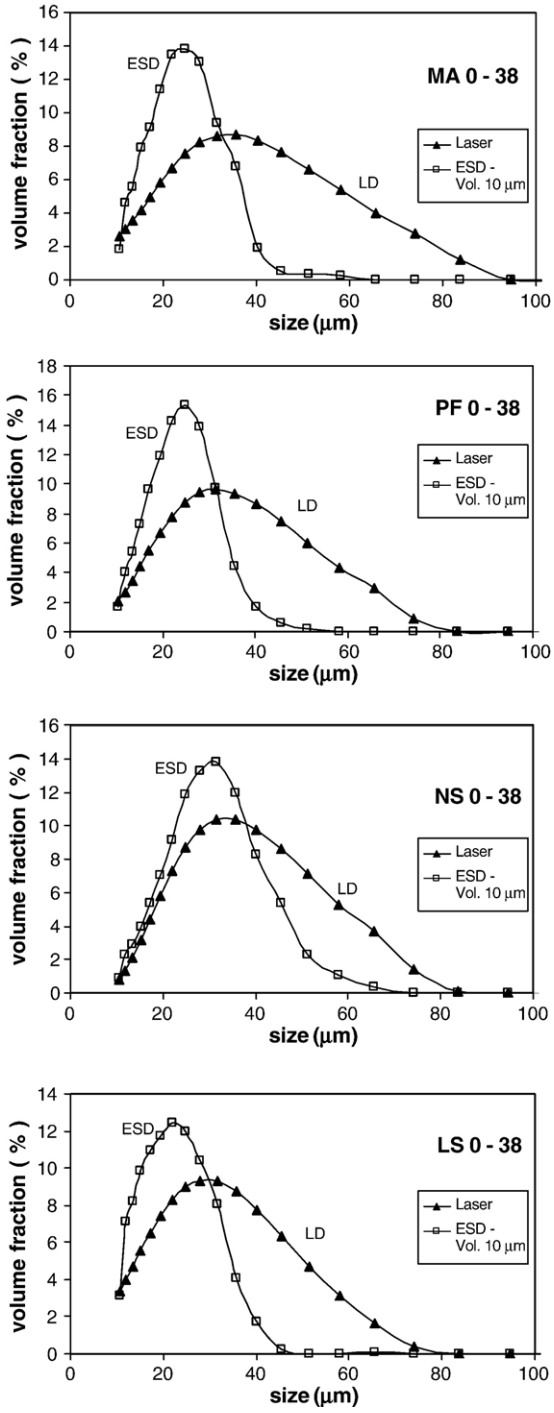

Fig. 3. PSD curves from laser diffraction (LD) and μCT–ESD for the 0 μm to 38 μm data.

ellipsoid of revolution. In the case of prolate ellipsoids, they found that the diffraction pattern was dominated by the long axis of the ellipsoidal particles. The PSD was roughly bimodal, with a more significant lower peak near the length of the minimum axis for the ellipsoid, and the higher peak at the orthogonal maximum axis length.

The PSDs for the four microfine aggregates used were also calculated using Fraunhofer theory and the resulting curves were essentially identical to the curves calculated using Mie theory, as the particles of interest are mostly sufficiently larger than the laser wavelength. Although aggregate particles do not have regular geometric shapes, it has been shown that particle shape can be successfully approximated using ellipsoids [15]. It can then be inferred that the LD PSD results will have a larger spread and a lower peak than the PSD curve for spherical particles of the same ESD, and naturally the μCT results. That is why using the L parameter, rather than the ESD parameter, brings better agreement between the μCT results and the LD results, since Ref. [25] showed that the longest particle length dominated the scattering results.

Fig. 3 shows the PSD curves measured using LD and μCT–ESD for the 0–38 microfines. The two curves agree or disagree with each other in a way similar to that of the 38 μm to 75 μm results in Fig. 3. We note that although particle agglomerates can be measured as single particles, we do not think that this played a role in any of the LD results since ultrasound was used to break up any agglomerates that might have been present. Increasing amounts of ultrasound did not change the results of the LD PSD measurements and dry LD measurements yielded similar results.

The μCT curves are cutoff at around 10 μm, since the smallest particle ESD from μCT was around 10 μm. LD, however, detected particles down to approximately 0.5 μm. The laser diffraction results were adjusted to include only particles larger than 10 μm, which means that the percentages of particles of larger sizes have been increased in order to keep the same normalization of the area under the curve. The LD results suggested that the different microfines contained 10% to 30% by volume of particles with ESD values below 10 μm.

4. Discussion

Non-spherical particle shape will definitely cause broadening in the LD PSD results, which are calculated from the laser diffraction scattering patterns assuming spherical shape particles. Using the measured shape statistics for the microfine aggregates, let us try to gain further insight into the LD results, focusing on the NS 38–75 results – the results for other microfines are analogous.

The NS 38–75 LD results were obtained on a sieved sample, so that nominally this sample had only particles in it between 38 μm and 75 μm in "size." Using the shape statistics for the NS 38–75 particles, this sieving can be examined more closely. What kind of particles can make it through these sieve classes? The complete listing of the L, W, and T parameters for the NS 38–75 particles are listed graphically in Fig. 4a, vs. the ESD that was calculated for each particle from its measured volume. It is interesting to observe the three bands formed by the L, W, and T data. In Fig. 4a, the overall trend or slope of the cloud of data points is dependent on average particle shape and size while the vertical variation of the width or length of particles with identical ESD indicates particle shape differences only.

LD PSD results are given in terms of an ESD value since, very simply put, LD collects two-dimensional projections to determine the diameter of an assumed spherical particle. This value of ESD is probably not determined in exactly the same way as the X-ray μCT

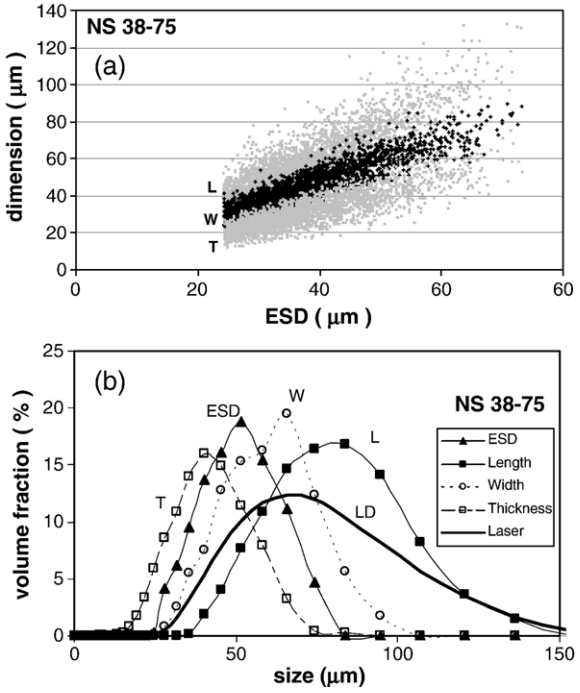

Fig. 4. (a) Principal dimensions (from μCT) of the NS 3875 particles plotted against their corresponding μCT–ESD values. (b) LD PSD results compared to various length parameters and ESD determined using μCT.

value of ESD is determined. However, it is instructive, using the μCT results, to examine what ESD values are reasonable, using Fig. 4a, to expect for particles that have passed a 75 μm sieve but have been retained on a 38 μm sieve. Particle width is the critical dimension in sieve analysis, since all particles in a size range need to have a width smaller than the maximum opening of the largest sieve through which they pass [35]. This is because two of a particle's dimensions must be smaller than the diagonal width of the square sieve opening in order for the particle to pass through. If the width of the particle fits through the sieve, then the thickness will as well, since by definition it is smaller than the width and is orthogonal to it. The length can be longer than this dimension. Therefore, particles in the NS 38–75 class must therefore definitely have widths less than $75 * 2^{1/2}$ μm ≈ 106 μm. Fig. 4a shows that all width values are less than about 90 μm, with a maximum ESD value of about 75 μm.

A quantitative analysis of the LD results for NS 38–75, shown in Fig. 4b, reveals that about 30% of the particles, by volume, have ESD values larger than 75 μm, and about 6%, by volume, have ESD values larger than 105 μm, which does not agree at all with the width results shown in Fig. 4a and the analysis just given, which has to hold for sieved particles. However, it was seen in Ref. [25] that for non-spherical objects, the apparent upper ESD limit of LD is determined by the longest axis of the objects. One could roughly say that the upper ESD limit of LD results depends on the longest particle axis, and the lower ESD limit of LD results depends on the shortest particle axis. The maximum length of a particle with ESD=75 μm, based on the μCT results in Fig. 4a however, is about 140 μm, which agrees fairly well with the upper limit of the LD results.

It is also seen in Fig. 4a that there are particles with width smaller than 38 μm, the smallest dimension of the opening of the sieve on which the material was supposed to be retained. All the NS 38–75 particles should ordinarily have widths exceeding this value, according to an analysis similar to that just given, but for the NS 38–75 microfine sample, about 15% by volume of the particles according to LD or about 12% according to μCT width, were incorrectly retained. While it is not very probable that particles with widths greater than the maximum opening of the top sieve for a size class be present in that size class, it is possible for particles with widths smaller than the minimum opening of the bottom sieve in a size to be retained on this bottom sieve. This could easily happen due to clogging of sieve openings and insufficient sieving time. This results in the μCT PSD curve to spread towards smaller sizes reducing the percentages of particles of larger sizes.

Two more factors that are related to each other and that possibly played a small role in creating the differences between the μCT and the LD results are sample size and sample statistics. The PSD curves obtained from μCT are exact for the particles measured, within the limits of the resolution of the original images. Several thousand particles were scanned and analyzed for each type of microfine aggregate. In LD, using a wet procedure, approximately 0.1 g of particles were used. If the relative density of the aggregates were about 2.5, a reasonable assumption, then 0.1 g would have a volume of 40 mm^3. If we assume average spherical particle size ranging from 38 μm to 75 μm, then there would be approximately 1.4 million to 175 000 particles in this size powder sample, so the numbers of particles used in the two methods are quite different. There would be even more particles in smaller particle size samples. So sample size statistics could perhaps have played some role, but probably a minor one, compared to the shape effects seen above. Another factor, which could not be controlled, is that the actual particle samples were both drawn from the same lot but were different for the two techniques. It was assumed, as mentioned previously, that the two samples of a certain microfine type were identical. This was almost certainly a very minor factor, since new lots of particles were drawn consistently from the same original lot by sampling from several locations to assure randomness. This assumption is always made in industrial practice since the use of large quantities of aggregates of a certain source in different concrete mixtures is based on characterization of a small sample of the aggregate.

One last point should be made about X-ray μCT voxel size. Much of this data was originally obtained at a voxel size of 4 μm, while the data reported here was taken at a voxel size of 2 μm. We obviously would like to get as small a voxel size as possible, near the wavelength of the red laser light used in the LD apparatus (about 0.7 μm). We don't have data for voxel sizes less than 2 μm; however, we can compare the 4 μm and 2 μm results to see if voxel size reduction mattered at all for these two sizes. If it did not, then a reduction of voxel size lower than 2 μm would probably not change the results significantly. Table 4 shows a comparison between the shape histograms for the MA 38–75 particles for the 2 μm and 4 μm voxel size μCT results. Note that the lower limit on the ESD, as calculated from the μCT results, was 48 μm. This is because the lower limit on

Table 4
Comparison between the shape histograms for the MA 38–75 particles for the 2 μm and 4 μm voxel size μCT results

4 μm voxels, 48 μm<ESD<74 μm					
$\mathcal{W}$ 5	0.0	0.0	0.0	0.0	0.0
$\mathcal{W}$ 4	0.0	0.0	0.0	0.0	0.0
$\mathcal{W}$ 3	0.0	0.0	0.2	0.0	0.0
$\mathcal{W}$ 2	0.0	3.3	1.7	0.4	0.0
$\mathcal{W}$ 1	53.6	36.4	4.0	0.2	0.0
2 μm voxels, 48 μm<ESD<74 μm					
$\mathcal{W}$ 5	0.0	0.0	0.0	0.0	0.0
$\mathcal{W}$ 4	0.0	0.0	0.0	0.0	0.0
$\mathcal{W}$ 3	0.0	0.0	0.0	0.0	0.0
$\mathcal{W}$ 2	0.0	5.8	2.2	0.7	0.0
$\mathcal{W}$ 1	55.5	32.8	2.9	0.0	0.0
	$\mathcal{L}$ 1	$\mathcal{L}$ 2	$\mathcal{L}$ 3	$\mathcal{L}$ 4	$\mathcal{L}$ 5

the 4 μm results, in terms of voxel size, was about 1000 voxels, in order to get reasonable shape results for a particle. This lower limit then directly translates to the ESD lower limit. But within these limits, it appears that voxel size does not change the shape results much at all. Similar results were obtained for the NS 38–75 particles. We did not have clear data sets at both size scales for the other particles considered in this study. We therefore conclude that going to an even lower voxel size would not help explain any differences between μCT and LD results.

5. Conclusion

The application of X-ray microtomography to determining the three-dimensional shapes and PSD of microfine aggregates was described, with guidelines for proper specimen preparation. Microtomography, in combination with the spherical harmonic method, allows the approximate calculation of the principal dimensions, volume, surface area, and other useful shape parameters for individual particles.

Three-parameter shape models, used for relating the physical dimensions of aggregates to their geometric properties, were used on four types of 38 μm to 75 μm microfines (several thousand particles of each). The model using a rectangular parallelepiped with dimensions determined from the principal moments of volume of the particles was shown to yield excellent linear correlations, with slopes near unity, of predicted vs. measured (with μCT) volume and surface area.

The length-to-thickness and width-to-thickness aspect ratios were calculated for particles of the two sizes of four different microfines and it was observed that the aspect ratios were similar. Shape histograms were calculated for the four microfine types and again by this measure the shape distributions were similar for the four aggregate types. The average aspect ratios for the <38 μm samples was slightly lower than those for the four 38 μm to 75 μm samples, but probably within experimental error. However, these averages only included particles greater than about 24 μm ESD, due to the minimum voxel size needed to be able to accurately determine the spherical harmonic coefficients for a given particle, so the averages for the entire <38 μm samples might be different if they would include much smaller particles.

Comparison of PSD curves measured using μCT to those measured with LD showed that using the L (length) parameter to characterize the size of the particles seemed to produce better agreement with the LD curves. In fact, it appeared, after qualitative and quantitative analysis of the particle dimensions, that the width of the LD PSD curve is well-approximated by having a lower limit determined by the minimum thickness of the particles (T) and an upper limit determined by the maximum length (L) of the particles. LD is a fast and simple way of obtaining PSD with very little sample preparation required. However, the effect of asphericity of the particles must be considered when using the measured PSD results or surface area estimates based on the PSD measurement and the assumption of spherical particle shape.

Acknowledgements

The X-ray μCT scans of the microfine aggregates were carried out at the National Synchrotron Light Source, Brookhaven National Laboratory, which is supported by the U.S. Department of Energy, Division of Materials Sciences and Division of Chemical Sciences, under Contract No. DE-AC02-98CH10886. We thank various industrial members of the International Center for Aggregate Research for supplying the microfine aggregates.

References

[1] J.F. Douglas, E.J. Garboczi, Intrinsic viscosity and polarizability of particles having a wide range of shapes, Advances in Chemical Physics 91 (1995) 85–153.
[2] E.J. Garboczi, K.A. Snyder, J.F. Douglas, M.F. Thorpe, Geometrical percolation threshold of overlapping ellipsoids, Physical Review E 52 (1995) 819–828.
[3] E.J. Garboczi, J.F. Douglas, Intrinsic conductivity of objects having arbitrary shape and conductivity, Physical Review E 53 (1996) 6169–6180.
[4] M.L. Mansfield, J.F. Douglas, E.J. Garboczi, Intrinsic viscosity and the electrical polarizability of arbitrarily shaped objects, Physical Review E 64 (2001) 61401–61416.
[5] E.J. Garboczi, J.F. Douglas, R.B. Bohn, A hybrid finite element-analytical method for determining the intrinsic elastic moduli of particles having moderately extended shapes and a wide range of elastic properties, Mechanics of Materials 38 (2006) 786–800.
[6] A.K.H. Kwan, C.F. Mora, Effects of various shape parameters on packing of aggregate particles, Magazine of Concrete Research 53 (2) (April 2001) 91–100.
[7] I. Ishai, E. Tons, Concept and test method for a unified characterization of the geometric irregularity of aggregate particles, Journal of Testing and Evaluation 5 (1) (1977) 3–15.
[8] S.S. Jamkar, C.B.K. Rao, Index of aggregate particle shape and texture of coarse aggregate as a parameter for concrete mix proportioning, Cement and Concrete Research 34 (11) (Nov. 2004) 2021–2027.
[9] E.D. Sneed, R.L. Folk, Pebbles in the Lower Colorado River, Texas — a study in particle morphogenesis, Journal of Geology 66 (2) (1958) 114–150.
[10] T. Fletcher, C. Chandan, E. Masad, K. Sivakumar, Aggregate imaging system for characterizing the shape of fine and coarse aggregates, Transportation Research Record 1832 (2003) 67–77.
[11] Reprinted from Innovations in Portland Cement Manufacturing, Chapter 10.3, in: J.I. Bhatty, F.M. Miller, S.H. Kosmatka (Eds.), Portland Cement Association, 5420 Old Orchard Road, Skokie, IL 60077, 2004, pp. 1311–1331.

[12] C.F. Ferraris, V.A. Hackley, A.I. Aviles, C.E. Buchanan Jr., NISTIR, vol. 6883, U.S. Department of Commerce Technology Administration, May 2002.
[13] M.A. Taylor, E.J. Garboczi, S.T. Erdoğan, D.W. Fowler, Some properties of irregular 3-D particles, Powder Technology 162 (2) (2006) 1–15.
[14] E.J. Garboczi, Three-dimensional mathematical analysis of particle shape using X-ray tomography and spherical harmonics: application to aggregates used in concrete, Cement and Concrete Research 32 (10) (Oct. 2002) 1621–1638.
[15] S.T. Erdoğan, P.N. Quiroga, D.W. Fowler, H.A. Saleh, R.A. Livingston, E.J. Garboczi, P.M. Ketcham, J.G. Hagedorn, S.G. Satterfield, Three-dimensional shape analysis of coarse aggregates: methodology and preliminary results on several different coarse aggregates, Cement and Concrete Research 36 (9) (Sept. 2006) 1619–1627.
[16] E.J. Garboczi, Tying Together Theory and Tests via Virtual Testing, Stone, Sand, and Gravel Review, Jan.–Feb. 2006, pp. 10–11, Available in Electronic Monograph, http://ciks.cbt.nist.gov/monograph/, Part I, Chapter 10, Section 6.
[17] E. Masad, S. Saadeh, T. Al-Rousan, E.J. Garboczi, D. Little, Computations of particle surface characteristics using optical and X-ray computed tomography images, Computational Materials Science 34 (2005) 406–424.
[18] D.W. Luerkens, Theory and Application of Morphological Analysis: Fine Particles and Surfaces, CRC Press, Boca Raton, Florida, 1991.
[19] E.N. Landis, E.N Nagy, D.T. Keane, Microstructure and fracture in three dimensions, Engineering Fracture Mechanics 70 (7–8) (2003) 911–925.
[20] J. Chotard, M.P. Boncoeur-Martel, A. Smith, J.P. Dupuy, C. Gault, Application of X-ray computed tomography to characterize the early hydration of calcium aluminate cement, Cement & Concrete Composites 25 (1) (2003) 145–152.
[21] N. Burlion, D. Bernard, D. Chen, X-ray microtomography: application to microstructure analysis of a cementitious material during leaching process, Cement and Concrete Research 36 (2) (Feb 2006) 346–357.
[22] C.M.G. Heffels, D. Heitzmann, E.D. Hirleman, B. Scarlett, The use of azimuthal intensity variations in diffraction patterns for particle-shape characterization, Particle and Particle Systems Characterization 11 (3) (Jun 1994) 194–199.
[23] Z.H. Ma, H.G. Merkus, B. Scarlett, Extending laser diffraction for particle shape characterization: technical aspects and application, Powder Technology 118 (1–2) (Aug. 2001) 180–187 (Sp. Iss. SI).
[24] P. Coppens, L. Deriemaeker, R. Finsy, Shape and size determination by laser diffraction: feasibility of data analysis by neural networks, Particle and Particle Systems Characterization 17 (3) (Oct 2000) 117–125.
[25] H. Mühlenweg, E.D. Hirleman, Laser diffraction spectroscopy: influence of particle shape and a shape adaptation technique, Particle & Particle Systems Characterization 15 (4) (1998) 163–169.
[26] A.C. Kak, M. Slaney, Principles of Computerized Tomographic Imaging, SIAM, New York, 2001.
[27] J.H. Dunsmuir, X-ray Microtomography, Guidebook to Imaging and Microspectroscopy at the NSLS, May 2002, http://www.nsls.bnl.gov/newsroom/publications/otherpubs/imaging/workshopdunsmuir.pdf.
[28] M.A. Taylor, Quantitative measures for shape and size of particles, Powder Technology 124 (2002) 94–100.
[29] H.C. van de Hulst, Light Scattering by Small Particles, New York, 1981.
[30] G. Mie, Beiträge zur Optik trüber Medien, speziell kolloidaler Metallösungen, Annalen der Physik (Leipzig) 25 (1908) 377–445.
[31] J. Cooper, Sizing up the Composition, Materials World 6 (1) (January 1998) 5–7.
[32] H. Goldstein, Classical Mechanics, Addison-Wesley, 1950.
[33] J.G. Stewart, Correlating Characteristics of Minus No.200 Fine Aggregate to Concrete Performance, M.S. Thesis, The University of Texas at Austin, 2005.
[34] J.K. Norvell, Prediction of concrete performance based on characteristics of minus no. 200 fine aggregate, M.S. Thesis, The University of Texas at Austin, 2005.
[35] J.M.R. Fernlund, The effect of particle form on sieve analysis: a test by image analysis, Engineering Geology 50 (1) (September 1998) 111–124.
[36] H. Volten, O. Muñoz, E. Rol, J.F. de Haan, W. Vassen, J.W. Hovenier, K. Muinonen, T. Nousiainen, Scattering matrices of mineral particles at 441.6 nm and 632.8 nm, Journal of Geophysical Research 106 (2001) 17375–17401.